TEKNIK, 46 (3), 2025, 306-316

## The Analysis of Target Drone Wing Sweep Angle on Dynamic Stall Condition with Pitch Rate Variation using Computational Fluid **Dynamics**

### Muhammad Agung Bramantya\*, Gesang Nugroho

Department of Mechanical and Industrial Engineering, Faculty of Engineering, Universitas Gadjah Mada Jl. Grafika No. 2, Kampus Teknik UGM, Yogyakarta, Indonesia 55281

Submitted: May 29th, 2025; Revised: June 28th, 2025; Accepted: July 19th, 2025; Available online: July 31st, 2025 DOI: 10.14710/teknik.v46i3.54148

### Abstract

A target drone is a type of Unmanned Aerial Vehicle (UAV) with a special mission as a shooting target in the military field. Target drones must be able to fly at high speeds and be agile. This study discusses the influence of the wing sweep angle on the aerodynamic performance of a target drone during dynamic stall conditions. Banshee Whirlwind-like model is used as a research object in this study with the adjustment of the empennage design to a V-Tail configuration. Furthermore, the wing sweep angle was varied to determine its effect on dynamic stall conditions using Computational Fluid Dynamics (CFD) in transient conditions. The wing sweep angle variations used were 5°, 20°, 35°, and 50°, whereas the dynamic stall condition was varied using pitch rates of 3.6%, 6%, and 18%. The aerodynamic performance discussed relates to the lift force, drag force, efficiency, stall angle, lateral stability, and stall development phase. The results of this study indicate that a wing sweep angle of 50° is the most optimal design in terms of stall condition, stability, and maneuverability.

**Keywords:** target drone, wing sweep angle, pitch rate, CFD, transient.

### 1. Introduction

The development of technology in the military field aligns with the increasing need for defense. The application of new technologies in the military sector is increasingly diverse, ranging from the Internet of Things, and Artificial Intelligence to automation systems. Air defense automation systems are widely used for weapons such as guided missiles and drones and represent the largest market share in the United States (Miller & Chadwick, 2018). One of the functions of crewless aircraft in the military field is as a target drone with a special mission as a shooting target, either during training or on the battlefield. Target drones have several advantages, especially in terms of safety. This is because the target drone does not require a crew to operate; therefore, it is suitable for use as a shooting target (Zhu et al., 2013) and (Banu et al., 2016). In addition, the size of the target drone can be adjusted according to the mission because it is not fixed in the cockpit space for the pilot.

optimal design.

performance. (Yen & Hsu, 2007) conducted a study using an experimental method with a wind tunnel to observe the flow separation structure on a swept-back wing. From the study results, a bubble burst occurred at a reasonably high

The target drone is a UAV with a fixed-wing configuration and the basic capabilities of flying at high

speed and maneuvering agilely. This ability aims to avoid

enemy attacks in each battle (Carter et al., 2011). To meet

the needs of its mission, the wing configuration must be

considered during the design stage. Based on the position

of the wing relative to the fuselage, it is divided into three

configurations: high, middle, and low. The low-wing

configuration is the most suitable for meeting the requirements of fast flight and good maneuverability

(Anderson, 1984), (Lan & Roskam, 2016), and

(Gundlach, 2012). Furthermore, the wing planform must

be considered to improve the aerodynamic performance.

One of the most suitable wing planforms for high speeds

is the swept-back wing (Sadraey, 2012). The sweep angle

on the wing must be investigated to obtain the most

conducted to determine its effect on the aerodynamic

Several studies on the wing sweep angle have been

\*) Corresponding Author E-mail: bramantya@ugm.ac.id

doi: 10.14710/teknik.v46i3.54148 Copyright © 2025, TEKNIK, p-ISSN: 0852-1697, e-ISSN: 240-9919

AoA of 20°. They continued their research, (Yen & Huang, 2009) investigated the effect of wing sweep angle variations on its aerodynamic performance using the same method as the previous study. The results show that the larger the wing sweep angle used, the stall angle will shift to 35° at the 45° wing sweep angle. Furthermore, (Bramantya et al., 2017) using the CFD method, examine the effect of the incidence angle and sweep angle on the wing on the coefficient of lift and coefficient of drag. The results show that a large wing sweep angle reduces CL at the same AoA. The dynamic stall condition was analyzed by Wang et al. (2021) on a 2D model of the NACA 0012 airfoil to observe the evolution of the vortex occurrence under stall conditions. The results show that dynamic stall is indicated by a development phase, which is classified into the attached flow stage stall development stage, onset stall, post-stall stage, and flow reattachment stage. Dynamic stall must be considered when the flow separation on the wing is delayed by rapid variations in the pitch rate under unsteady conditions (Choudhry et al., 2014), (Carr, 1985), and (Visbal & Benton, 2018). These studies only discussed the wings, whereas the interference of the wings with the fuselage affected the performance. Thus, a complete model of the target drone was developed in this study.

The use of a sweep angle on a target drone provides a stall delay, which is very useful for maneuvering under extreme conditions. The sweep-back angle provides an even distribution of lift, such that stall conditions occur in the tip chord area and propagate to the chord root area (Sadraey, 2012). This allows the lift to remain awake for a longer period. The dynamic stall condition on the wing sweep angle has not been discussed in several previous studies; therefore, we will explore its application to existing target drone models in this study.

The CFD method was used in this study. This method has advantages in terms of ease and significant development cost savings (Versteeg & Malalasekera, 2007). The use of turbulent models must be considered to provide accurate results in the simulation. For transient conditions, detached eddy simulation is the most suitable turbulent model considering the computational load that can be reduced but still improve the turbulent flow prediction in regions with significantly separated flows (Neves et al., 2020) and (Zhou et al., 2019).

In this study, a target drone with wing sweep angle variation was simulated under operational conditions and models already on the market. The AHP and WDM methods were used to determine the target drone model. Furthermore, the CFD method will simulate the planned flight conditions. The simulation results for lift force, drag force, efficiency, stall angle, lateral stability, and stall development phase are discussed to obtain a target drone design with the most optimal wing sweep angle.

A comprehensive review clarified the LEV onset and reattachment mechanisms relevant to ramp pitching (Gardner et al., 2023), whereas high-fidelity studies on swept finite wings linked the increased sweep to stall delay and spanwise vortex transport (Hammer et al., 2021). Numerical investigations have further identified leading-edge sweep as a primary driver of aerodynamic performance and vortex organization (Aleisa et al., 2023). Methodological advances, such as UDF-based dynamicstall evaluation frameworks, align with our unsteady CFD approach (Sterpu et al., 2024), and recent studies have related the sweep and reduced frequency to the LEV topology, reinforcing our sweep-dependent trends (Cavanagh et al., 2024). Complementary UAV/airframe optimization studies emphasize sweep-mission tradeoffs.

### 2. Material and Methods

The target drone model used was the Banshee Whirlwind-like model offered by QinetiQ, with the main missions being air-to-air missiles, ground-to-air missiles, and gun systems (QinetiQ, 2020). This target drone has an engine with a power of 40 bhp static thrust and a rotary engine type with a pusher configuration. The target drone was equipped with multiple smoke and infrared tracking flares. With a take-off system using a launcher and landing using a parachute, the Banshee Whirlwind is suitable for use on land and sea. In this study, a Banshee Whirlwind-like model was used with empennage modifications using a V-tail configuration (Figure 1). Some specifications of the Banshee Whirlwind performance are listed in Table 1 (QinetiQ, 2020).

**Table 1** Specification of ISI Sky I

No.	Parameters	Capability Values	
1	Wingspan	2.49 m	
2	Length	2.85-2.95 m	
3	Wing area	2.42 m <sup>2</sup>	
4	Speed	46-100 m/s	
	range		
5	Launch	32 m/s	
	speed		
6	Endurance	>90 minutes	

The existing Banshee Whirlwind model has a wing sweep angle of 35°. Furthermore, the model was varied with sweep angles on the wings of  $5^{\circ}$ ,  $20^{\circ}$ , and  $50^{\circ}$  to determine the characteristics of each variation during dynamic stall conditions. The sweep angle used in this study was the angle between the wing quarter-chord line ( $\Lambda$ C/4). Wing models with variations in the sweep angles of  $5^{\circ}$ ,  $20^{\circ}$ ,  $35^{\circ}$ , and  $50^{\circ}$  are shown in Figure 2.

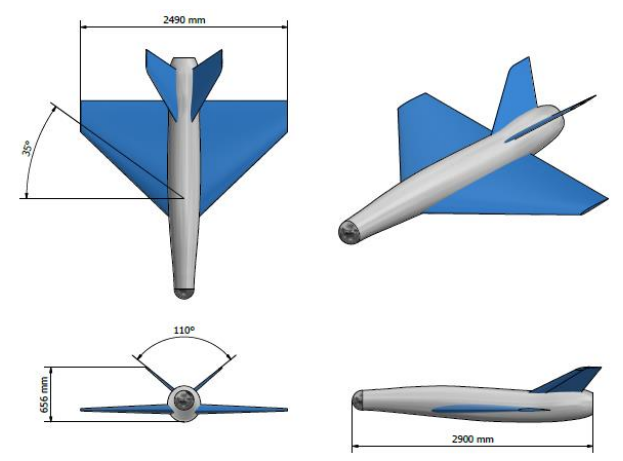
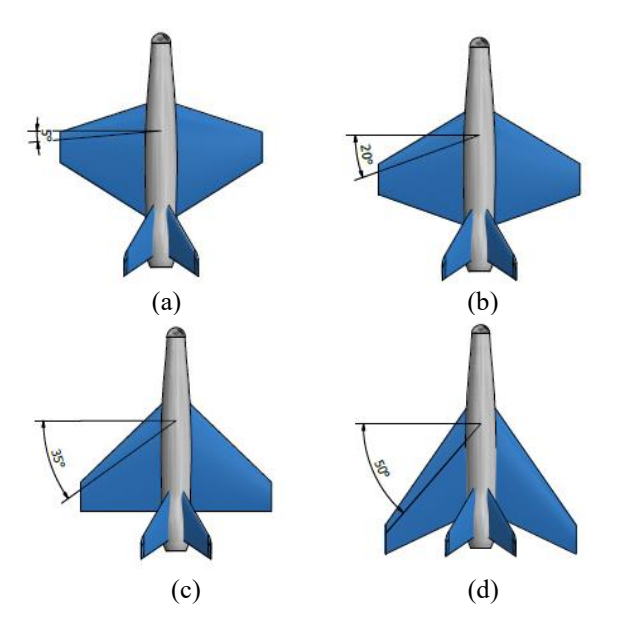


Figure 1 The Banshee Whirlwind-like dimension



**Figure 2** Model variations, (a) wing sweep angle 5°, (b) wing sweep angle 20°, (c) wing sweep angle 35°, (d) wing sweep angle 50°.

CFD modeling was used to evaluate the aerodynamic performance based on the influence of wing sweep angle variations on dynamic stall conditions. CFD-based numerical simulations will be completed using ANSYS Fluent 2020 R2 available at the Laboratory of Heat and Mass Transfer, Gadjah Mada University (Wibowo et al., 2019) and (Mukaarim, 2021). CFD software solves several governing equations used in modeling fluid flow. The CFD method will be used to solve the unsteady Detached-Eddy Simulation (DES) equation. The CFD method consists of three stages: preprocessing, solving, and post-processing.

### 1. Pre-processing

At this stage, a fluid or computational domain was created. The fluid domain must represent the fluid flow area around the object by considering the effect of wall interference on the simulation. The dimensions of the fluid domain significantly affected the simulation results. A fluid domain that is too large will use a more significant computational load, whereas a fluid domain that is too small can disrupt the fluid flow around the object. The size of the fluid domain uses a reference that has been studied by (Wibowo et al., 2019). The fluid domain used in this study comprised two parts: the rotary and static domains. The rotary domain simulates the pitching movement to achieve dynamic stall conditions, with the rotational speed controlled by the pitch rate variation. Figure 3 shows the fluid domain used in this study.

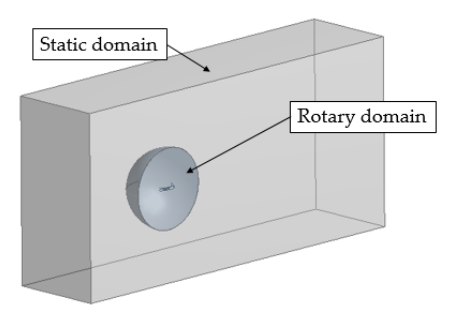


Figure 3 Fluid Domain

Furthermore, a meshing process is carried out to divide the continuous fluid domain into discrete computational domains. An unstructured polyhedral mesh, as shown in Figure 4, was used. A Grid Independence Test (GIT) was conducted to ensure that the addition of the number of meshes no longer affected the simulation results. The GIT results show that the mesh number of  $\pm 7.3$  million is the optimal value, as shown in Figure 5. The quality of the mesh can be achieved by applying inflation to the area around the object wall so that the skewness and orthogonal quality can be achieved according to the standards set by the ANSYS Fluent.



Figure 4 Computational Polyhedral Mesh

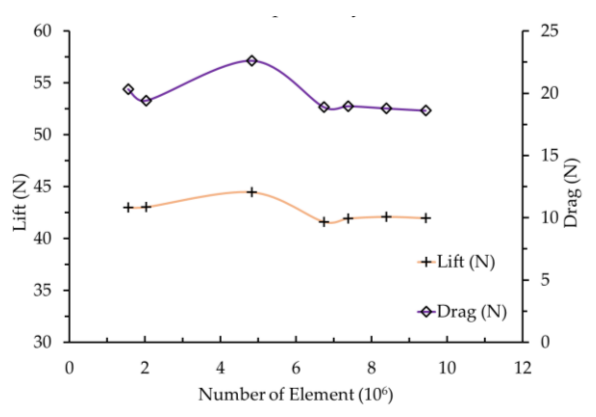


Figure 5 Grid Independency Test

### 2. Solving

This stage begins with determining the general model used, followed by determining the appropriate turbulence model. In this study, the DES turbulence model was used, which has several advantages, as discussed previously. The air material was conditioned to match the operational conditions of the target drone, which had a cruising altitude of 3000m. The air used was considered incompressible because the simulation was performed at Mach numbers below 0.3. The pitch rate variations will use values of 3.6°/s, 6°/s, and 18°/s. The solver conditions are presented in Table 2.

Table 2 Solver condition

General			
Solver type	Pressure-based		
Time	Transient		
Model			
Viscous model	k-omega SST		
Cell Zone Condition			
Mesh motion	Pitch rate variation		
Material			
Fluid	Air (density 0,9093 kg/m³)		
Boundary Condition			
Inlet	Velocity-inlet		
Outlet	Pressure-outlet		
Symmetry	Symmetry		
Wall	No-slip condition		
Solution Method			
Pressure-velocity coupling	SIMPLE with		
Pressure-velocity coupling	second-order		
Calculation			
Number of time step	900		
Timo ston sizo	Based on pitch		
Time step size	rate		
Max iteration/time step	50		

### 3. Post-processing

This stage is used to observe the simulation results and retrieve the required data. These results can be visualized as two- or three-dimensional images using ANSYS CFD-Post software. In addition, the results of the computational calculations are also in the form of numbers, which can then be processed in Microsoft Excel software to display the data in tables or graphs.

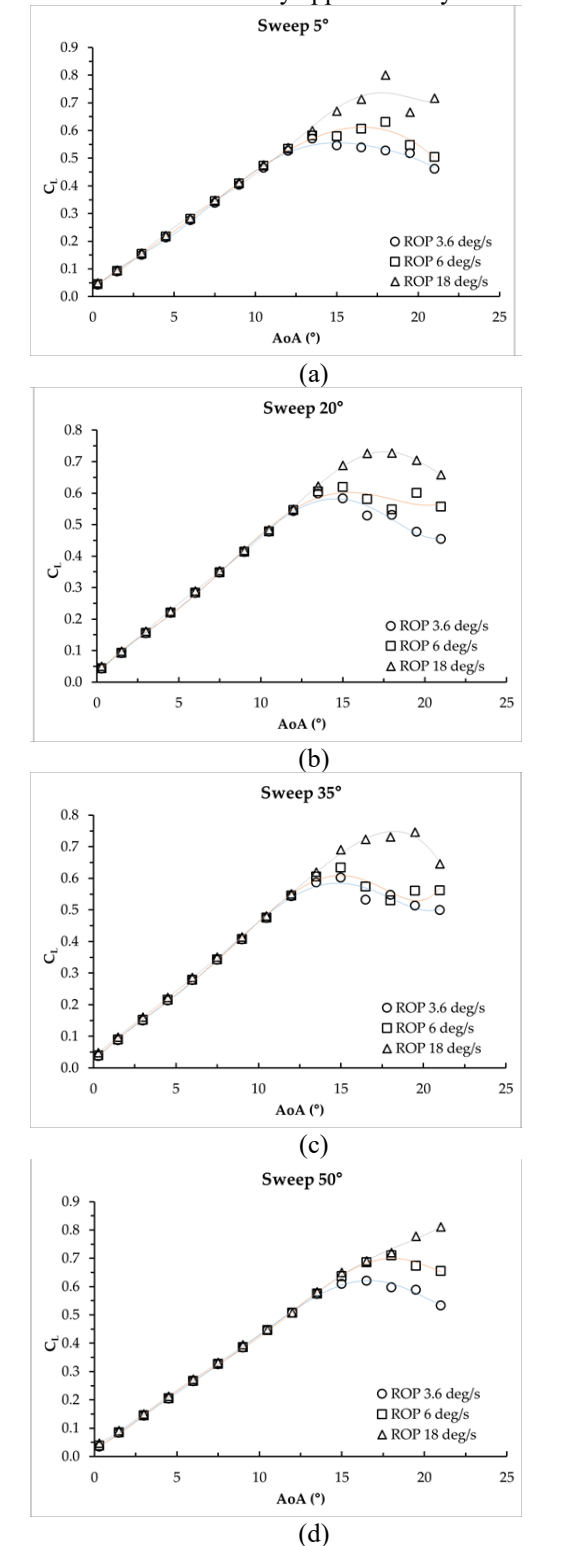
### 3. Results

## 3.1. The Effect of Pitch Rate Variation on Aerodynamic Performance

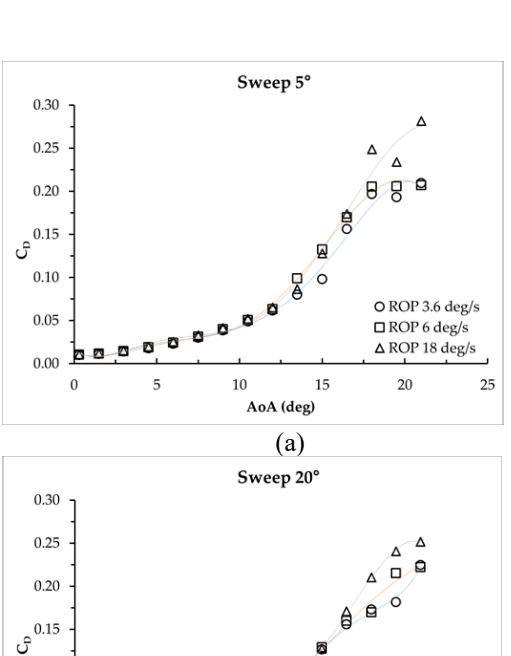
As mentioned earlier, several parameters related to aerodynamic performance are discussed in this study. The aerodynamic performance included CL, CD, and CL/CD under transient conditions based on variations in the pitch rate. Data in the form of graphs were used to represent the aerodynamic performance of the drone target. The effect of pitch rate variation on a certain wing sweep angle is discussed in this section based on its aerodynamic performance. The goal was to determine how dynamic conditions affect the aerodynamic performance of a target drone under pitching conditions. Figure 6 shows the graph of CL against AoA at various pitch rates. The results show that the greater the pitch level used, the greater the CL when approaching stagnant conditions. Conditions with a higher pitch rate also create a stall that occurs at a larger AoA, such that an increase in the pitch rate will delay the occurrence of a stall. The most significant increase in CLMAX occurred at a sweep angle of 50°, approximately 14.5%, owing to the rate of pitch increase, whereas at sweep angles of 35°, 20°, and 5°, the CLMAX increase was 5.3 %, 3.3 %, and 2 %, respectively. . Increasing the pitch rate also delayed stalling at sweep angles of 50°, 35°, 20°, and 5°by approximately 3°, 4°, 3°, and 4.5°, respectively, from the condition with the lowest pitch rate  $(3.6^{\circ}/\text{ s})$ .

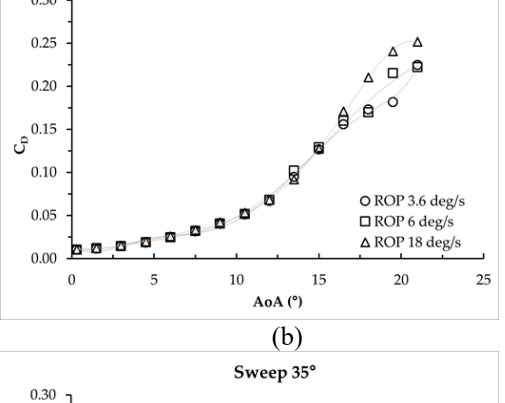
Figure 7 shows the value of CD with respect to AoA for the target drones with variations in the pitch rate. Consequently, there was no significant difference at low AoAs in the CD value owing to an increase in the pitch rate. However, when the AoA approaches a jammed condition, the CD value increases, and there is a significant difference between the tone levels used. This increase in pitch rate variations resulted in higher CD values under kiosk conditions. The increases in the CD values for variations in the sweep angles of 50°, 35°, 20°, and 5° were 84%, 64%, 36%, and 23%, respectively. To determine which pitch rate variation is the most effective, the efficiency represented by the CL/CD value is considered. From Figure 8, we can see that the maximum efficiency obtained at AoA is approximately 5° with a low pitch rate condition, which has a higher value. This implies that lower pitch levels are more efficient for use

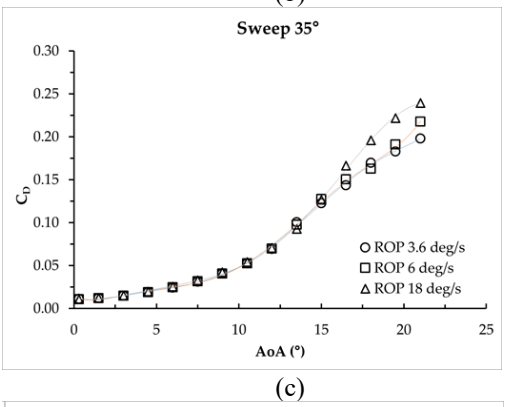
at low AoA and vice versa. The decline in CL/CDMAX for all variations decreased by approximately 0.6%.



**Figure 6** CL vs AoA for wing sweep angle: (a) 5°, (b) 20°, (c) 35°, and (d) 50°.







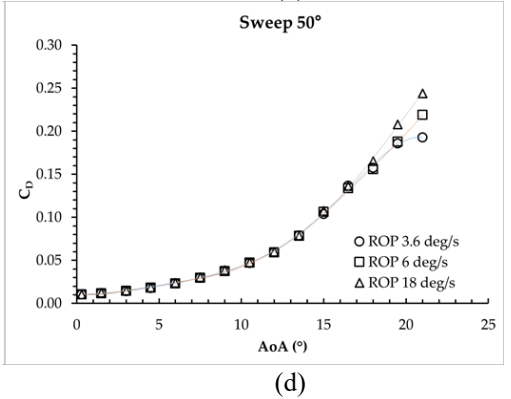
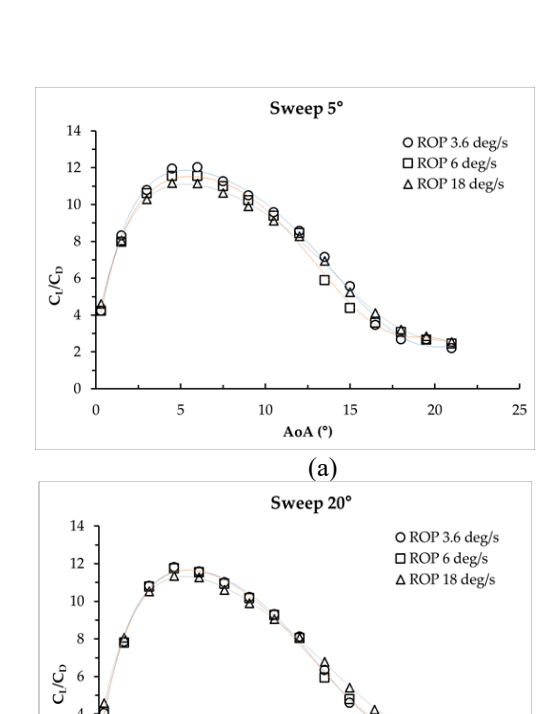
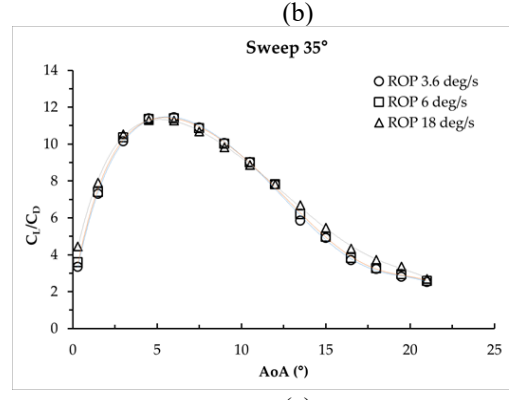


Figure 7 CD vs AoA for wing sweep angle: (a)  $5^{\circ}$ , (b)  $20^{\circ}$ , (c)  $35^{\circ}$ , and (d)  $50^{\circ}$ .

25

20





AoA (°)

0

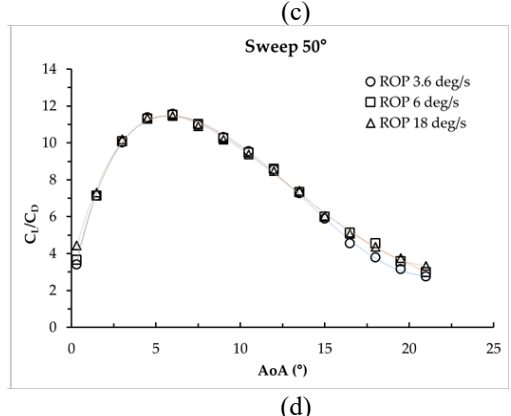


**Figure 8** CL/CD vs AoA for wing sweep angle: (a) 5°, (b) 20°, (c) 35°, and (d) 50°.

# 3.2. The Effect of Wing Sweep Angle Variation on Aerodynamic Performance

In this section, we compare the variations of the wing sweep angle on the aerodynamic performance at certain pitch rate variations. The goal was to determine the optimal sweep angle for use at various pitch speeds. Figure 9 shows the value of C<sub>L</sub> with respect to time for various pitch variations. The results show that the larger the sweep angle used, the larger the CLMAX at all pitch rate variations. In addition, the increase in the C<sub>LMAX</sub> value also resulted in a higher AoA delay, although this was not significant. On average, the increase in C<sub>LMAX</sub> ranged from 2%-6%. From the C<sub>D</sub> value in Figure 10, there was no significant difference between the wing sweep angle variations at all pitch rate variations. This means that for maneuvering at high pitch rates, a significantly different power is not considered so that the pitch rate does not affect the power requirements of the target drone. The efficiency is shown by the C<sub>I</sub>/C<sub>D</sub> value in Figure 11, and the results show that a smaller wing sweep angle is more efficient at low AoA and vice versa.

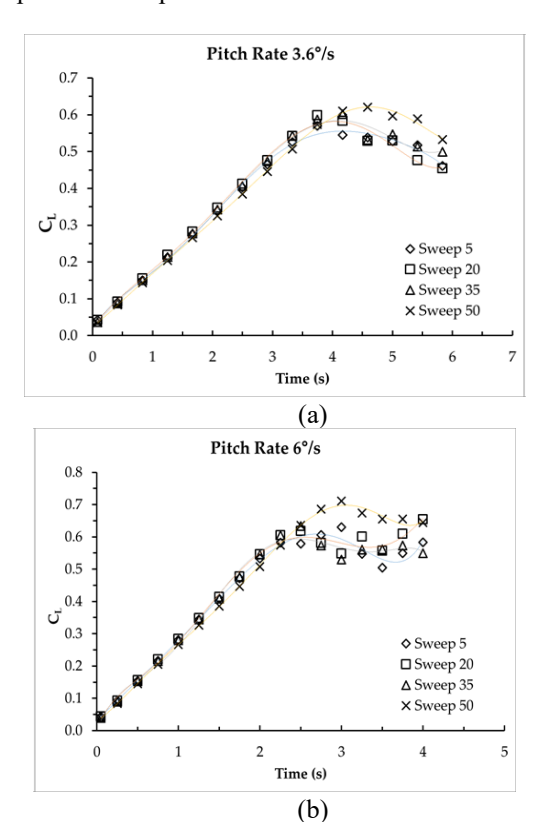
Beyond the lift/drag trends, the 50° sweep exhibits stability-relevant features that justify its recommendation under the target drone's high-AoA, rapid-pitch envelope. Longitudinally, the delayed root-proximal separation and re-phasing of the leading-edge vortex (LEV) reduce abrupt nose-up pitching moments at stall onset, yielding a smoother post-stall moment evolution and stronger pitch rate damping during ramp maneuvers. This behavior is consistent with a more benign dynamic-stall cycle and a wider controllable AoA window, which, operationally, supports a robust pitch-control authority near the performance boundary.

Laterally and directionally, a higher sweep enhances an effective dihedral-like response and promotes the spanwise convection of separated structures toward the tip, mitigating sudden root-anchored asymmetries that degrade roll controllability. Wing-body coupling at 50° also shifts the peak suction and load distribution to preserve aileron effectiveness deeper into the maneuver, whereas the swept planform's inherent weathercock tendency supports directional stability during transient sideslip. Taken together, these longitudinal and lateral tendencies align with the mission need for aggressive, yet controllable, high-AoA maneuvering, thereby strengthening the selection of a 50° sweep.

Large sweep angles introduce nontrivial structural and sustainability implications. A 50° planform typically requires higher torsional stiffness, refined load paths at the wing–fuselage junction, and tighter aeroelastic margins, which may increase the structural weight, joint count, and manufacturing precision. These features propagate to maintenance: more complex access around

spars, ribs, and control-linkage routing; stricter inspection for fatigue at root/junction regions; and potential increases in man-hours for non-destructive testing. Conversely, modular panelization, standardized fasteners, and composite layup tailoring can mitigate the recurring costs. Hence, the aerodynamic benefits at high AoAs must be balanced against the structural complexity and lifecycle burden, with maintainability considered a first-order design constraint.

From an autopilot perspective, the 50° sweep provides larger stability margins under rapid pitch and sideslip transients: delayed root separation and smoother Cm evolution reduce the phase lag and commandresponse overshoot, easing gain scheduling and improving disturbance rejection. Energy-wise, while highly swept wings may incur slightly higher drag at low AoA cruise (wetted-area/induced penalties), the configuration attenuates dynamic-stall excursions and roll-yaw coupling, lowering throttle transients and control-deflection power. Consequently, consumption and endurance depend on the mission's duty cycle. For target-drone profiles dominated by brief, high-AoA maneuvers, reduced oscillatory losses, and tighter trajectory keeping can offset cruise penalties, yielding comparable or improved endurance.



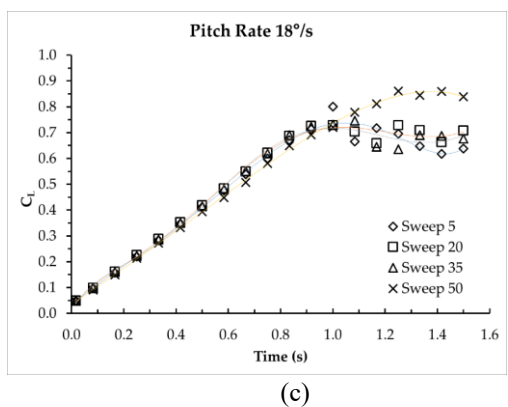


Figure 9 CL vs time for pitch rate variation: (a)  $3.6^{\circ}$ /s, (b)  $6^{\circ}$ /s, and (c)  $18^{\circ}$ /s.

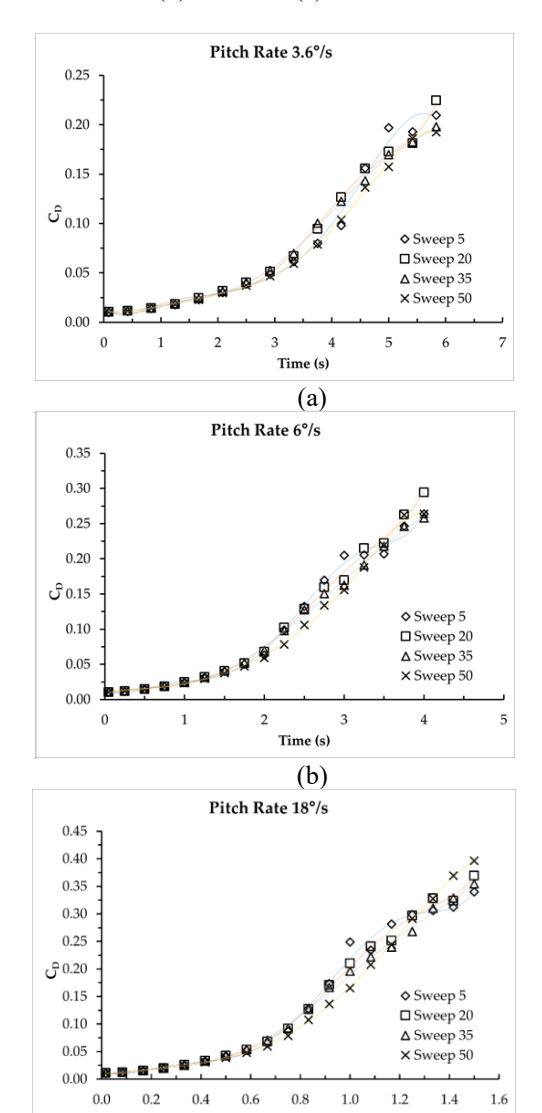


Figure 10 CD vs time for pitch rate variation: (a)  $3.6^{\circ}$ /s, (b)  $6^{\circ}$ /s, and (c)  $18^{\circ}$ /s.

(c)

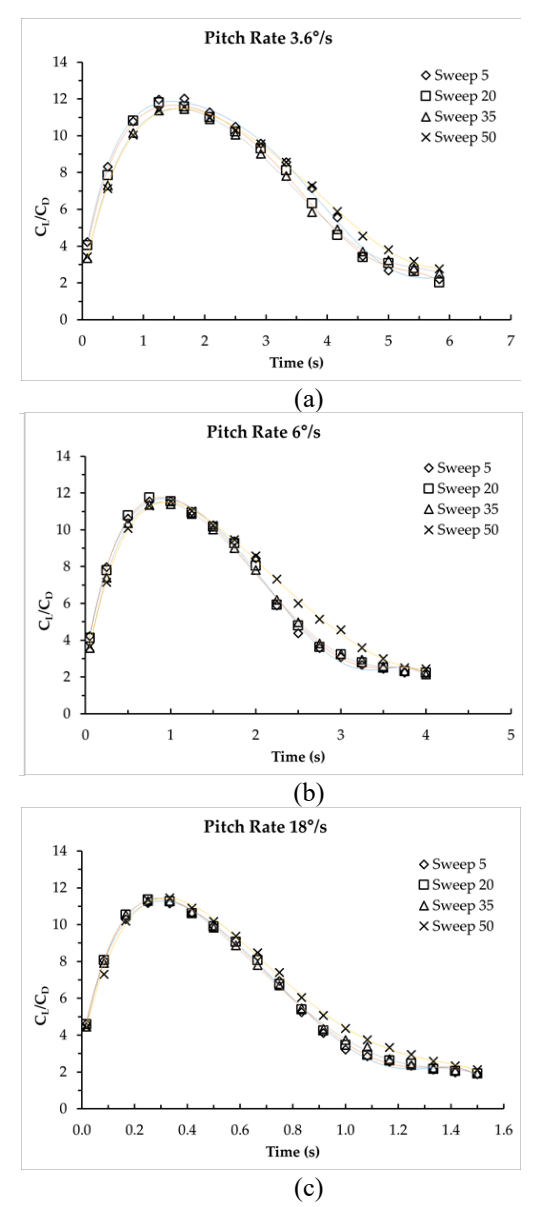


Figure 11  $C_L/C_D$  vs time for pitch rate variation: (a)  $3.6^{\circ}/s$ , (b)  $6^{\circ}/s$ , and (c)  $18^{\circ}/s$ .

### 3.3 The Development of Dynamic Stall

For the formation of flow separation due to the influence of dynamic stall, Figure 11 shows the process of flow separation on the target drone's airfoil cross-section. The contours are taken on the mean aerodynamic chord of the flank, that is, 495.5 mm extra from the root chord. In this discussion, an example of the stall development phase is taken at a variation of the wing sweep angle of 50° at a pitch speed of 6°/s. Initially, the flow separation appeared very thin in the trailing edge area, which is referred to as the stall development stage in Figure 11a. Then, the flow separation increased towards the leading edge, indicating that it had reached a

stall condition called stall onset, as shown in Figure 11b. The vortex enlarged and formed completely at the post-stall stage, as shown in Figure 11c. At this stage, a wake region appears in the area behind the wing with unstable lift force fluctuations. This condition is dangerous and difficult to recover using the control system. This built-up area interferes with the tail function of the target drone to regulate the pitching movements. The increasing AoA condition reaches the fully developed stall stage in Figure 11d, where the wake region fills the rear wing area, and the drone target loses lift significantly.

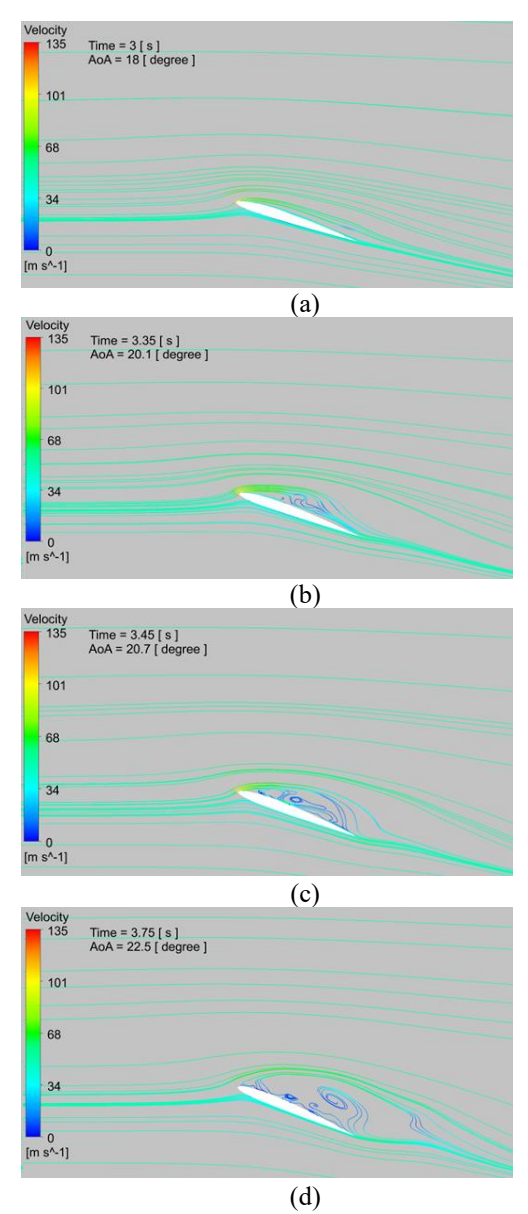


Figure 12  $C_L/C_D$  vs time for pitch rate variation: (a)  $3.6^{\circ}/s$ , (b)  $6^{\circ}/s$ , and (c)  $18^{\circ}/s$ .

This study aimed to determine the most optimal wing sweep angle based on the pitch level. The target drone was designed to have extreme flight capabilities at high AoA and fast movement response. This ability can be observed in its aerodynamic performance, represented by the values of CL, CD, CL/CD, and stall conditions. From the CL value, the optimal design for the target drone was chosen, which had the highest CLMAX with stall conditions that occurred at the highest AoA. This indicates that a target drone capable of flying with this capability can maneuver at extremely high AoA. The value of CD represents the amount of power required; therefore, the smaller the CD, the smaller the power requirement. In terms of efficiency, the use of a high AoA is often carried out when the drone target is operating, so that good efficiency in high AoA becomes the parameter design of a drone target.

Among the above parameters, the 50° sweep angle variation was the most optimal design because it met the performance requirements of the target drone. The 50° wing sweep angle had the highest stall angle with the highest CLMAX in both low and large pitch conditions. In addition, the 50° wing-sweep angle efficiency was the best under large AoA operating conditions. Therefore, the target drone design with a wing sweep angle of 50° is the most optimal to meet the existing requirements. The design of the target drone with a wing sweep angle of 50° is shown in Figure 12. To analyze the performance of the target drone more deeply, in-depth research can be conducted regarding stability in the longitudinal, lateral, and directional directions.

Wing-Fuselage Aerodynamic Interference (Full-Drone Model). Using the full-drone geometry introduces junction and forebody effects that reframe the dynamic stall sequence relative to an isolated wing. The fuselage alters the local incidence via forebody upwash, thickens the boundary layer along the sidewall, and generates a horseshoe vortex at the wing-body junction. These mechanisms modify the effective camber and loading near the root, thereby shifting the onset, strength, and spanwise migration of the leading-edge vortex (LEV) during ramp pitching. At a lower sweep, the combined upwash and junction vortex increase the effective angle of attack inboard, encouraging earlier root-proximal separation and a more uniform spanwise advance of the separation front. At higher sweep angles, stronger spanwise convection transported nascent LEV structures outboard, restraining root-anchored redistributing separated flow toward the mid-span and tip. Consequently, wing-fuselage coupling does not simply advance or delay stall; it re-phases the unsteady cycle and re-allocates the aerodynamic loading across the span. Practically, these interference effects influence the location of peak suction, with implications for aileron effectiveness and structural margins near the root, particularly in high-AoA maneuvers central to the targetdrone mission. The magnitude of the interference remains geometry- and Reynolds-dependent and may be further modulated by the propulsive slipstream and control deflections, both of which are beyond the scope of this study. Within these limits, the full-drone results rationalize the observed sweep-dependent differences and clarify the departures from the isolated-wing intuition.

Although we did not perform our own wind tunnel or flight tests, we benchmarked the CFD trends qualitatively against (Ullah et al., 2021) Ullah's tunnel study on pitching swept finite wings (0°, 15°, and 30°), which documented sweep-induced spanwise convection, modified LEV topology, and root-to-tip redistribution of separation during dynamic stall. Our 50° case extends this tendency: increased sweep delays root-anchored stall, smooths the pitching-moment evolution, and shifts peak loading outboard, consistent with Ullah's experimental observations of more benign unsteady behavior as the sweep increases. This alignment supports the reliability of our comparative conclusions for high AoA maneuvers. Dedicated wind tunnel experiments will be conducted in subsequent studies to provide quantitative validation.

### 4. Conclusion

study discusses the aerodynamic This performance of a target drone under dynamic conditions with variations in the pitch rate at varying wing sweep angles. This study used the CFD method to comprehensively observe the phenomena that occur under dynamic conditions and their effects on the aerodynamic performance. From the analysis of the values of CL, CD, CL/CD, and stall conditions, it was found that a wing sweep angle of 50° was the most optimal to meet the existing requirements because of its ability to maneuver at high stall angles with relatively the same power requirements. Although the present conclusions were drawn from unsteady CFD, they are consistent with wind tunnel observations of swept finite wings regarding sweep-induced spanwise convection, LEV phasing, and stall delay. These qualitative agreements support the comparative trends identified in this study, particularly for high-AoA maneuvers. A dedicated wind tunnel campaign using the same geometry and motion law is planned as the next step to provide quantitative validation and refine the design recommendations.

### References

Aleisa, H., Kontis, K., & Nikbay, M. (2023). Numerical Investigations on Low-Speed Aerodynamic Characteristics of Generic Unmanned Combat Aerial Vehicle Configurations. *Journal of Aircraft*, 60(6), 1965–1975. https://doi.org/10.2514/1.C037258

- Anderson, J. D. (1984). Fundamentals of Aerodynamics. https://api.semanticscholar.org/CorpusID:117923648
- Banu, T. P., Borlea, G. F., & Banu, C. (2016). The Use of Drones in Forestry. *Journal of Environmental Science and Engineering B*, 5(11). https://doi.org/10.17265/2162-5263/2016.11.007
- Bramantya, M. A., Nugroho, G., & Dimas, R. (2017). Pengaruh Sudut Swept dan Sudut Incidence pada Sayap Pesawat Tanpa Awak dengan Simulasi Komputasi Dinamika Fluida. *Prosiding SNTTM XVI*, 9–13.
- Carr, L. (1985, August 19). Dynamic stall progress in analysis and prediction. *12th Atmospheric Flight Mechanics Conference*. 12th Atmospheric Flight Mechanics Conference, Snowmass,CO,U.S.A. https://doi.org/10.2514/6.1985-1769
- Carter, D., Burris, P., Brandt, S., & Anemaat, W. (2011, September 20). Fifth-Generation Target Drone Project Initial Development. 11th AIAA Aviation Technology, Integration, and Operations (ATIO) Conference. 11th AIAA Aviation Technology, Integration, and Operations (ATIO) Conference, Virginia Beach, VA. https://doi.org/10.2514/6.2011-7011
- Cavanagh, A., Bose, C., & Ramesh, K. (2024). Effect of sweep angle on three-dimensional vortex dynamics over plunging wings. *Physics of Fluids*, *36*(11), 117115. https://doi.org/10.1063/5.0227012
- Choudhry, A., Leknys, R., Arjomandi, M., & Kelso, R. (2014). An insight into the dynamic stall lift characteristics. *Experimental Thermal and Fluid Science*, 58, 188–208. https://doi.org/10.1016/j.expthermflusci.2014.07.006
- Gardner, A. D., Jones, A. R., Mulleners, K., Naughton, J. W., & Smith, M. J. (2023). Review of rotating wing dynamic stall: Experiments and flow control. *Progress in Aerospace Sciences*, 137, 100887. https://doi.org/10.1016/j.paerosci.2023.100887
- Gundlach, J. (2012). Designing Unmanned Aircraft Systems: A Comprehensive Approach. American Institute of Aeronautics and Astronautics. https://doi.org/10.2514/4.868443
- Hammer, P. R., Garmann, D. J., & Visbal, M. R. (2021, August 2). Effect of Aspect Ratio on Swept Wing Dynamic Stall. *AIAA AVIATION 2021 FORUM*. AIAA AVIATION 2021 FORUM, VIRTUAL EVENT. https://doi.org/10.2514/6.2021-2948
- Lan, C. E., & Roskam, J. H. (2016). *Airplane Aerodynamics and Performance*. https://api.semanticscholar.org/CorpusID:61127642
- Miller, C., & Chadwick, S. (2018). *Military Unmanned Aerial Vehicles and Diversification Opportunities*. https://doi.org/10.13140/RG.2.2.25777.02402
- Mukaarim, M. A. D. (2021). Perancangan Pesawat Tanpa Awak Berjenis Unmanned Aerial Target dan

- Simulasi Numerik Variasi Sudut Sweep pada Sayap terhadap Performa Aerodinamika [Universitas Gadjah Mada]. https://etd.repository.ugm.ac.id/penelitian/detail/201 145
- Neves, A. F., Lawson, N. J., Bennett, C. J., Khanal, B., & Hoff, R. I. (2020). Unsteady aerodynamics analysis and modelling of a Slingsby Firefly aircraft: Detached-Eddy Simulation model and flight test validation. *Aerospace Science and Technology*, *106*, 106179. https://doi.org/10.1016/j.ast.2020.106179
- QinetiQ. (2020). Banshee Whirlwind<sup>TM</sup> Uncrewed Aerial Target by QinetiQ. https://www.qinetiq.com/en/whatwe-do/services-and-products/banshee-whirlwind
- Sadraey, M. H. (2012). *Aircraft Design: A Systems Engineering Approach* (1st ed.). Wiley. https://doi.org/10.1002/9781118352700
- Sterpu, D.-A., Măriuţa, D., & Grigorie, L.-T. (2024). A UDF-Based Approach for the Dynamic Stall Evaluation of Airfoils for Micro-Air Vehicles. *Biomimetics*, 9(6), 339. https://doi.org/10.3390/biomimetics9060339
- Ullah, A. H., Tomek, K. L., Fabijanic, C., & Estevadeordal, J. (2021). Dynamic Stall Characteristics of Pitching Swept Finite-Aspect-Ratio Wings. *Fluids*, 6(12), 457. https://doi.org/10.3390/fluids6120457
- Versteeg, H. K., & Malalasekera, W. (2007). An introduction to computational fluid dynamics—The finite volume method. https://api.semanticscholar.org/CorpusID:29589033
- Visbal, M. R., & Benton, S. I. (2018). Exploration of High-Frequency Control of Dynamic Stall Using Large-Eddy Simulations. *AIAA Journal*, *56*(8), 2974–2991. https://doi.org/10.2514/1.J056720
- Wang, W., Cao, S., Dang, N., Zhang, J., & Deguchi, Y. (2021). Study on dynamics of vortices in dynamic stall of a pitching airfoil using Lagrangian coherent structures. *Aerospace Science and Technology*, 113, 106706. https://doi.org/10.1016/j.ast.2021.106706
- Wibowo, S. B., Sutrisno, & Rohmat, T. A. (2019). Study of Mesh Independence on the Computational Model of the Roll-up Vortex Phenomenon on Fighter and Delta Wing Models. *International Journal of Fluid Mechanics Research*, 46(5), 427–439. https://doi.org/10.1615/InterJFluidMechRes.2018025530
- Yen, S. C., & Hsu, C. M. (2007). Influence of Boundary Layer Behavior on Aerodynamic Coefficients of a Swept-Back Wing. *Journal of Fluids Engineering*, 129(6), 674–681. https://doi.org/10.1115/1.2734212
- Yen, S. C., & Huang, L. –C. (2009). Flow Patterns and Aerodynamic Performance of Unswept and Swept-Back Wings. *Journal of Fluids Engineering*, *131*(11), 111101. https://doi.org/10.1115/1.4000260

- Zhou, L., Gao, Z., & Du, Y. (2019). Flow-dependent DDES  $/\gamma R e^-\theta$  t coupling model for the simulation of separated transitional flow. *Aerospace Science and Technology*, 87, 389–403. https://doi.org/10.1016/j.ast.2019.02.037
- Zhu, K., Bo, Y., Tao, D., & Wang, J. (2013). Route design of the target drone. 2013 IEEE International Conference on Cyber Technology in Automation, Control and Intelligent Systems, 175–178. https://doi.org/10.1109/CYBER.2013.6705441